




Article

Quantification of the Seismic Behavior of a Steel Transmission Tower Subjected to Single and Repeated Seismic Excitations Using Vulnerability Function and Collapse Margin Ratio

Moustafa Moufid Kassem ¹, Salmia Beddu ^{2,*}, Wong Qi Min ¹, Chee Ghuan Tan ³
and Fadzli Mohamed Nazri ^{1,*}

¹ Engineering Campus, School of Civil Engineering, Universiti Sains Malaysia, Nibong Tebal 14300, Malaysia; moustafa.mk@usm.my (M.M.K.); wongqimin@student.usm.my (W.Q.M.)

² Department of Civil Engineering, Institute of Energy Infrastructure, Universiti Tenaga Nasional, Jalan Ikram-Uniten, Kajang 43000, Malaysia

³ Department of Civil Engineering, Faculty of Engineering, Universiti Malaya, Kuala Lumpur 50603, Malaysia; tancg@um.edu.my

* Correspondence: salmia@uniten.edu.my (S.B.); cefmn@usm.my (F.M.N.)

Abstract: Transmission towers are a vital lifeline for modern living and are crucial structures that must remain operational even after a seismic event. However, the towers are largely designed to withstand the effects of wind alone and not earthquakes, and the seismic influences on tower design and construction have hitherto been ignored. The purpose of this study was to evaluate the seismic performance of a latticed steel transmission tower-line system that is subjected to a variety of seismic situations (Far-Field, Near-Field and Repeated Earthquakes) using probabilistic vulnerability functions and Collapse Margin Ratios in accordance with FEMA-P695. Nonlinear Time History Analyses were performed by incorporating an array of 36 strong ground motions to develop the Incremental Dynamic Analysis and to generate the fragility functions for three performance limit states as referenced in FEMA 356. The results showed that the single event seismic performance of the tower is better than its performance after multiple ground motions owing to aftershock impact, while near-field excitations led to greater susceptibility and fragility than far-field scenarios. Thus, near-field ground motion is more harmful to the tower and could result in its failure or collapse with only a small reduction in damage relative to the impact of the aftershock.

Keywords: repeated earthquakes; vulnerability function; collapse margin ratio; incremental dynamic analysis; fragility curve



Citation: Kassem, M.M.; Beddu, S.; Qi Min, W.; Tan, C.G.; Mohamed Nazri, F. Quantification of the Seismic Behavior of a Steel Transmission Tower Subjected to Single and Repeated Seismic Excitations Using Vulnerability Function and Collapse Margin Ratio. *Appl. Sci.* **2022**, *12*, 1984. <https://doi.org/10.3390/app12041984>

Academic Editors: Linsheng Huo and Dongdong Chen

Received: 19 January 2022

Accepted: 8 February 2022

Published: 14 February 2022

Publisher's Note: MDPI stays neutral with regard to jurisdictional claims in published maps and institutional affiliations.



Copyright: © 2022 by the authors. Licensee MDPI, Basel, Switzerland. This article is an open access article distributed under the terms and conditions of the Creative Commons Attribution (CC BY) license (<https://creativecommons.org/licenses/by/4.0/>).

1. Introduction

Modern societies rely on tower-based transmission systems to provide electricity, the vital lifeline, to their citizens. When an earthquake strikes, damage and failure of transmission towers can result in significant economic losses, as well as delays in post-seismic rehabilitation. To withstand seismic shocks, transmission towers, which are the most critical load-bearing structures in this system, must have exceptional earthquake resistance to ensure their continued operation. Despite this, seismic loads are not taken into consideration in design codes and guidelines and many transmission towers have historically failed and even collapsed during earthquakes [1,2].

An important example of an earthquake-induced failed transmission line was during the Landers earthquake of 1992, in which about 100 transmission lines and several transmission towers failed in the city of Los Angeles [3]. The 1995 Kobe earthquake in Japan destroyed half the transmission lines in the area and about 20 transmission towers were rendered tilted due to the movement of the earthquake's epicentre [4]. Similarly, the Chi-Chi earthquake of 1999 in Taiwan caused significant damage to electric power

systems. A total of 69 transmission lines were destroyed, 15 transmission towers collapsed, and 26 transmission towers tilted. The Wenchuan earthquake of 2008 in China caused the collapse of more than 20 transmission towers in the Mao County area, as well as the destruction of a 220 kV transmission line in the region [5–7]. The Kocaeli earthquake in Turkey in 1999 induced landslides, faulting, and surface ruptures, thus damaging many of the transmission towers [4]. Figure 1 shows the collapsed transmission towers caused by the Wenchuan earthquake in 2008.

The transmission steel tower is typically designed by considering the wind effects as the primary source of the lateral loads with no attention paid to seismic effects. This is because wind lateral loads are thought to be much greater than seismic lateral loads on high-rise transmission towers, particularly in open areas. However, earthquake effects on towers may be more severe than wind effects and seismic lateral load cannot be ignored, particularly in high-seismic zones, because seismic lateral loads can also cause significant damage to the transmission and telecommunication steel towers. Thus, design checks, even if simple ones, must be incorporated to account for seismic-event induced lateral load [8]. It is also imperative to perform a vulnerability assessment on transmission steel towers that have been subjected to earthquakes.

There have been few studies on the evaluation of earthquake-related tower performance [9–15]. Fernández Lorenzo et al. [16] used static equivalent and dynamic time history methods to compare the structural response of a self-supported communication tower in terms of internal forces and displacements under hurricane wind conditions. Rezayibana [17] studied the effect of soil type on seismic response of the stiff and ductile part of tall telecommunication towers with random vibration analysis. In the modelling and analysis, various conditions of the soil under the tower and various damping conditions were used. Tsavdaridis, et al. [18] proposed using structural topology optimization to develop solutions for lattice self-supported telecommunication towers in terms of weight-to-stiffness ratio. Chandra and Sengupta [19] presented a comparative study of self-supporting telecommunication towers using dynamic analysis for optimum modal combination and discretization. Szafran et al. [20] used tensioned joint reliability to estimate the reliability of slender steel lattice telecommunication towers by a full-scaled pushover test of a 40 m tall lattice tower.

Several codes, standards and design provisions have proposed simplified static methods for the seismic estimation for transmission steel towers [21–23], but none of the norms have suggested using the non-linear dynamic analysis (NL-DA) approach. This provision demonstrates the gaps and limitations in estimating seismic design capability. Furthermore, since the transmission lines spans are large in modern civil engineering construction, the effects of multiple excitations must be carefully considered, and the frequent failures of transmission line tower systems show that the load pattern defined in the codes does not accurately reflect realistic load conditions [24].

Due to the aforementioned limitation gap in the proposed provisions, this research is undertaken to conduct a non-linear dynamic analysis to understand and estimate the load pattern in transmission line towers. A non-linear time history analysis (NL-THA) technique is used to estimate the tower Collapse Margin Ratio (CMR) and the probability of damages is calculated using vulnerability functions. The CMR was originally proposed by FEMA P-695, as one of the best structural collapse indicators established in the last decade [25]. According to FEMA P-695, various factors influence the CMR, including ground motion variability and uncertainty in the structure's design, analysis, and construction. These variables are combined in a collapse fragility curve, which describes the likelihood of the seismic-force-resisting system collapsing as a function of ground motion intensity related to FEMA P-695 [26]. The CMR is an effective tool for determining the capability of a structure to withstand structural collapse.

Thirty-six ground motion records comprising 18 far-field (FF) and 18 near-field (NF) earthquakes are used to simulate two types of earthquakes that have different characteristics and involve different behaviours in structures [27]. Near-field earthquakes occur in fields

close to the fault, while far-field earthquakes occur in fields far from the fault. For instance, some researchers propose a near-field range of 10 to 60 km around the fault [28]. On the other hand, some international code standards define the site-to-source distance less than 15 km as the near-field, while the far-field range can be described as a distance greater than 15 km from the epicentre of an earthquake.

The properties of far-field ground motions are different from near-field ground motions. When compared to higher frequencies of far-field ground motions, near-field ground motions have higher acceleration and more restricted frequency range [28]. Furthermore, far-field ground motion is less disruptive and devastating than near-field ground motion [29]. This could imply that far-fault ground motions are less likely than near-field ground motions to cause transmission steel tower failure or even collapse. Consequently, it is critical to assess the vulnerability of transmission steel towers in both far-field and near-field ground motions, in order to reduce the risk of tower failure or collapse during an earthquake and keep the tower operational after the event. Furthermore, the collapse of a tower can be avoided by ensuring better seismic code compliance in new constructions and rehabilitating existing structures.



Figure 1. Collapsed transmission towers in China caused by the Wenchuan earthquake [30].

To date, there have been few studies that have evaluated the vulnerability of lattice transmission steel towers under the influence of the Far-Field (FF), Near-Field (NF), and repeated ground motions. In this study, the seismic performance of a steel transmission tower is evaluated for three different seismic scenarios; such analysis will be useful in updating the code regulations and demonstrating that it is dangerous to ignore seismic effects on transmission towers.

2. Structure Prototype and Finite Element Model

2.1. Description of the Structural Prototype Layout

A typical 220 kV transmission tower is assumed to be located in Lebanon, which is designed for seismic hazard with Peak Ground Acceleration (PGA) of 0.25 g corresponding to the exceeding probability of 10% in 50 years. It can be observed from the contour map in Figure 2a that the PGA in the Lebanese territory has fluctuated during a 50-year period, ranging from 0.2 g in the eastern part of the nation to 0.30 g in the western part of the country near the coastal districts in the east [31]. Several surrounding seismic sources can increase the seismic vulnerability of Lebanon structures and infrastructures facilities as shown in Figure 2b; (1): The Dead Sea fault (2): Ghab- fault: A line source is also modelled stretching from the northern Lebanese border into the North of Syria, with a total length of 124 km. (3): The Karasu area source, covering 29,000 km². This mostly comprises

earthquakes along the eastern branch of the Anatolian fault system in Turkey, (4): The Eastern Syrian regions comprise a total size of around 4300 km², (5): Cyprus region is an area source with a surface size of approximately 70,000 km². It comprises seismic activity on and around the island of Cyprus [32].

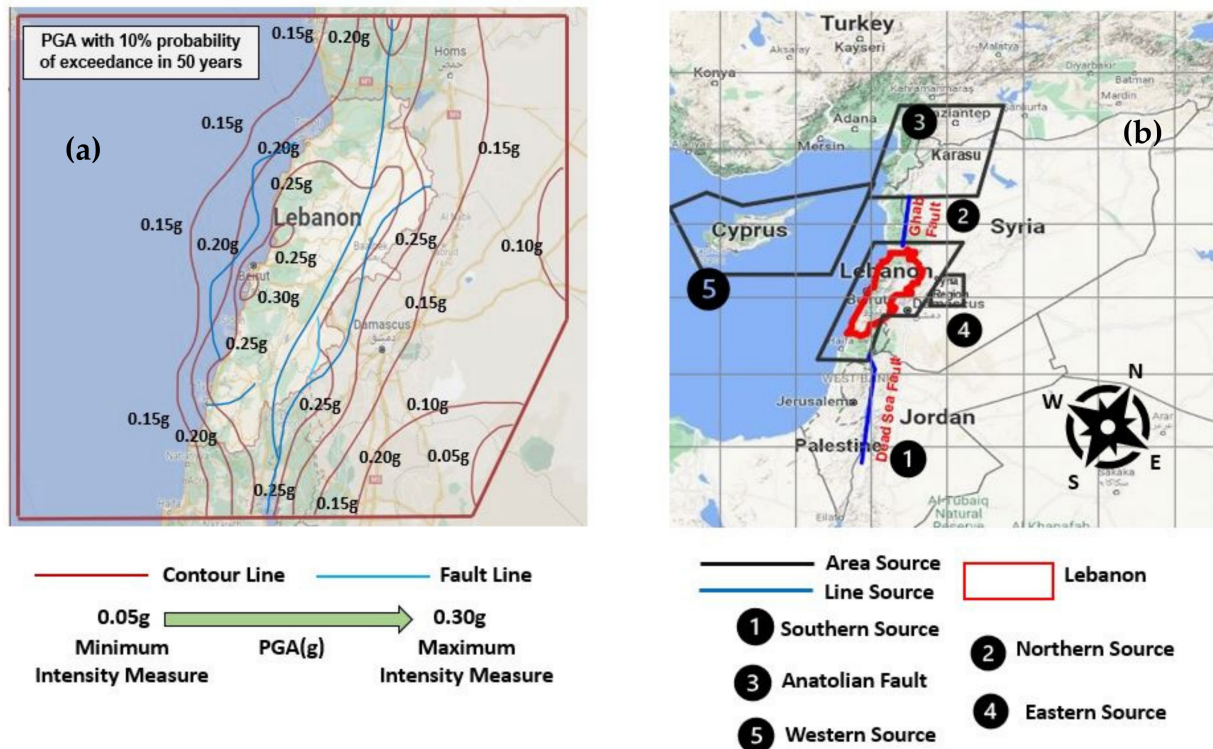


Figure 2. Lebanese seismic norm, (a): Contour map of PGA with 10% possibility of occurrence in 50 years, (b): Lebanon border by seismically active sources.

The selected tower is designed as a Diamond Lattice Bracing system with an angle tower “Type A” denoted by a suspension tower with a line deviation of 0° to 2° according to ASTM standards. This particular tower was chosen because it is one of the most frequently encountered forms. The geometrical cross-sectional used for the tower are steel angles made from A 992/A 992M, according to ASTM standard specification for structural steel alloy [33].

The finite element computer program SAP2000 is utilised to model the investigated TL system, which consists of three transmission towers. The two transmission line spans are assumed to have the same height of 42.95 m with a 300 m span distancing between each tower and the tower is assumed to weigh approximately 20 t. In addition, it consists of three crossarms at elevations of 29.85 m, 33.95 m, and 38.05 m, denoted as the bottom, middle and top crossarms, respectively, and the lengths of the three crossarms are 6.20 m, 8.30 m and 5.70 m, respectively. The model is composed of 922 members (beam, bracing and columns) and 568 nodes with rigid connections between members. The base of the tower is permanently fastened to the ground and is 4.0 m wide at the base. There are 14 transmission lines, including two ground lines that are connected at the top tower, and 12 transmission conductors are suspended at the cantilever crossarms’ ends as shown in Figures 3 and 4. Table 1 lists the characteristics of the conductors and ground wires. There is also comprehensive information regarding the sizes of the component steel members in the towers, in which the transmission tower’s geometry and cross-sectional details are shown in Table 2 and labelled in Figure 4. The transmission steel tower material is designed according to the ASTM A 992/A 992M for each frame member as shown in Table 3.

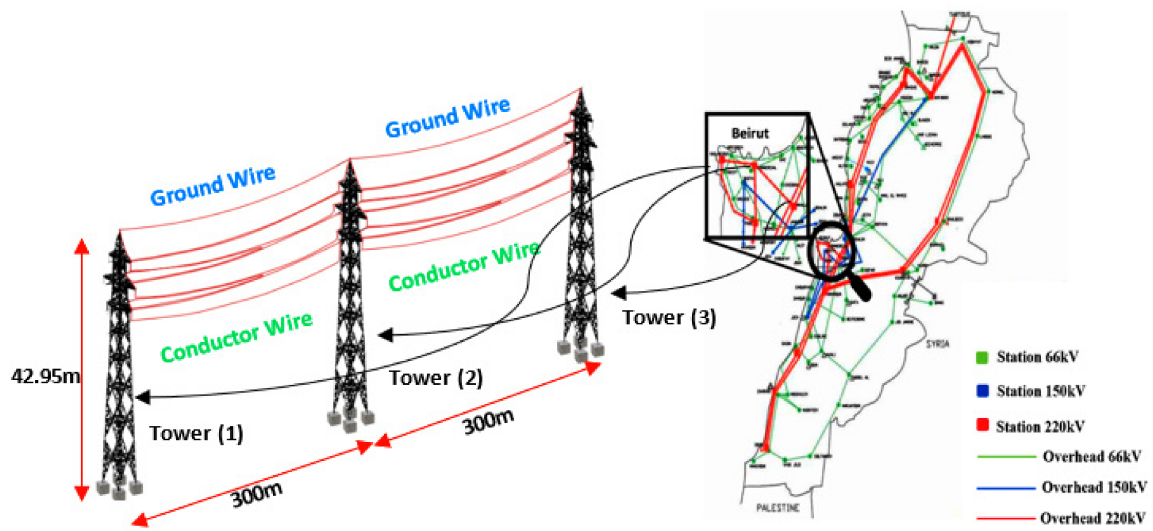


Figure 3. Sketch of 3D- finite element model of the symmetrical selected transmission tower line in Beirut.

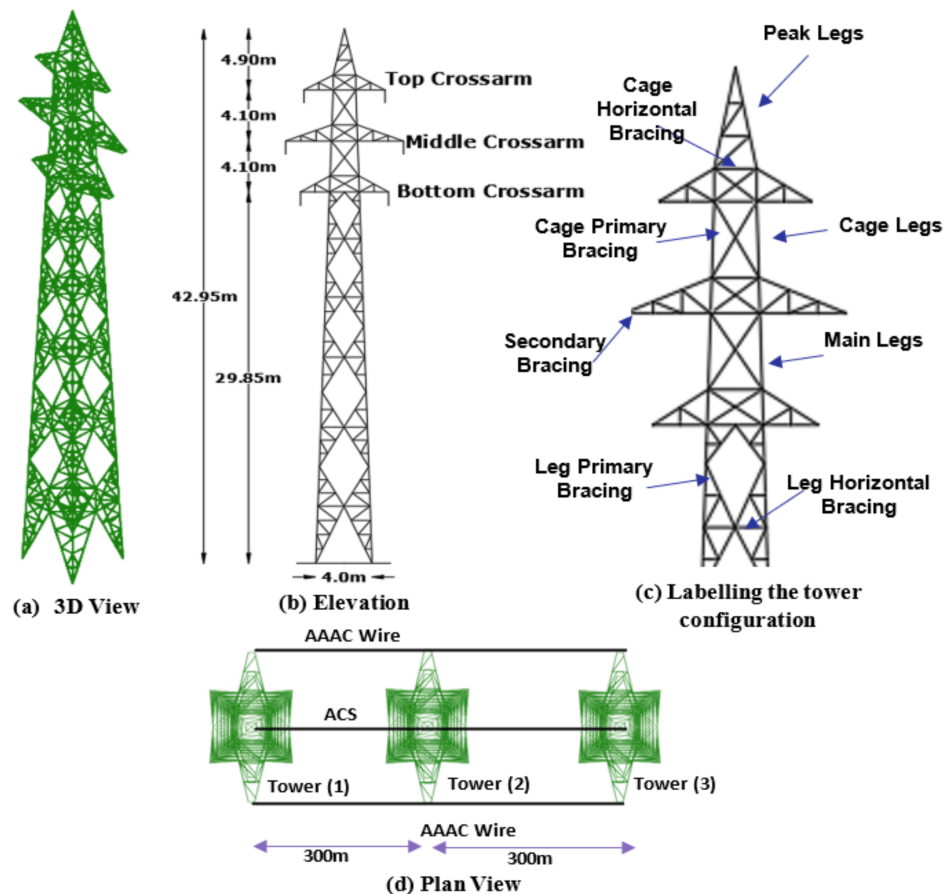


Figure 4. The geometrical design of lattice tower with a voltage of 220 kV.

Table 1. Mechanical characteristics of the conductor lines and ground wires.

Items	Conductor Lines	Overhead Ground Wires
Type	AAC (Aluminum Alloy Conductor)	ACS (Aluminum Clad Steel)
Name	Aster 570	ASTM
Section (mm ²)	570.22	77.55
Overall diameter (mm)	31.05	11.5
Unit weight (kg/m)	1.574	0.472
Modulus of elasticity (GPa)	56	140
Coefficient of linear expansion/°C	23.0×10^{-6}	13.9×10^{-6}

Table 2. List of member profiles used in this study.

Section	Profile Size (mm)	Unit Weight (N/m)	Area (mm ²)
Peak Legs	L60 × 60 × 5	44.83	581.9
Cage Legs	L120 × 120 × 11	195.22	2537
	L150 × 150 × 14	310	4004
Cage Primary Bracing	L50 × 50 × 5	36.99	480.3
	L70 × 70 × 7	72.50	939.7
	L80 × 80 × 7	83.28	1082
	L100 × 100 × 10	147.54	1900
Cage Horizontal Bracing	L60 × 60 × 5	44.83	581.9
	L70 × 70 × 7	72.50	939.7
	L80 × 80 × 7	83.28	1082
	L100 × 100 × 8	119.49	1551
Top Cross Arm	L60 × 60 × 5	44.83	581.9
	L80 × 80 × 10	116.35	1511
Middle Cross Arm	L70 × 70 × 6	62.69	812.7
	L100 × 100 × 10	147.54	1915
Bottom Cross Arm	L60 × 60 × 6	53.17	684
	L80 × 80 × 7	83.28	1082
Main Legs	L150 × 150 × 14	310.00	4004
	L180 × 180 × 16	426.74	5504
	L180 × 180 × 18	476.77	6191
	L200 × 200 × 18	531.70	6911
	L200 × 200 × 20	587.91	7635
Leg Primary Bracings	L100 × 100 × 8	119.49	1551
	L100 × 100 × 10	147.54	1900
	L100 × 100 × 12	174.91	2271
	L120 × 120 × 11	195.22	2537
Leg Horizontal Bracings	L60 × 60 × 5	44.83	625
	L70 × 70 × 6	62.69	812.7
	L80 × 80 × 7	83.28	1082
Secondary Bracings	L35 × 35 × 3	15.70	203.7
	L40 × 40 × 4	23.74	307.9
	L45 × 45 × 4	26.98	349.3
	L60 × 60 × 5	44.83	581.9

Table 3. Material Properties of ASTM A 992/A 992M.

Property	Symbol	Value
Modulus of Elasticity	E	199,948 MPa
Shear Modulus	G	76,903 MPa
Poisson’s Ratio	ν	0.3
Tensile Yield Strength	Fy	345 MPa
Tensile Ultimate Strength	Fu	448 MPa

2.2. 220 kV Transmission Line Loading

Without proper tower loading, towers are worthless. The most critical aspect of tower design is the loading on the tower. The transmission tower design in this study considers the loading calculations on the tower, which are made in accordance with the ASCE standard [34]. The loadings considered are dead load, wind load, and seismic load (time history analysis). Figure 5 describes the structural loading terms and their directional conventions.

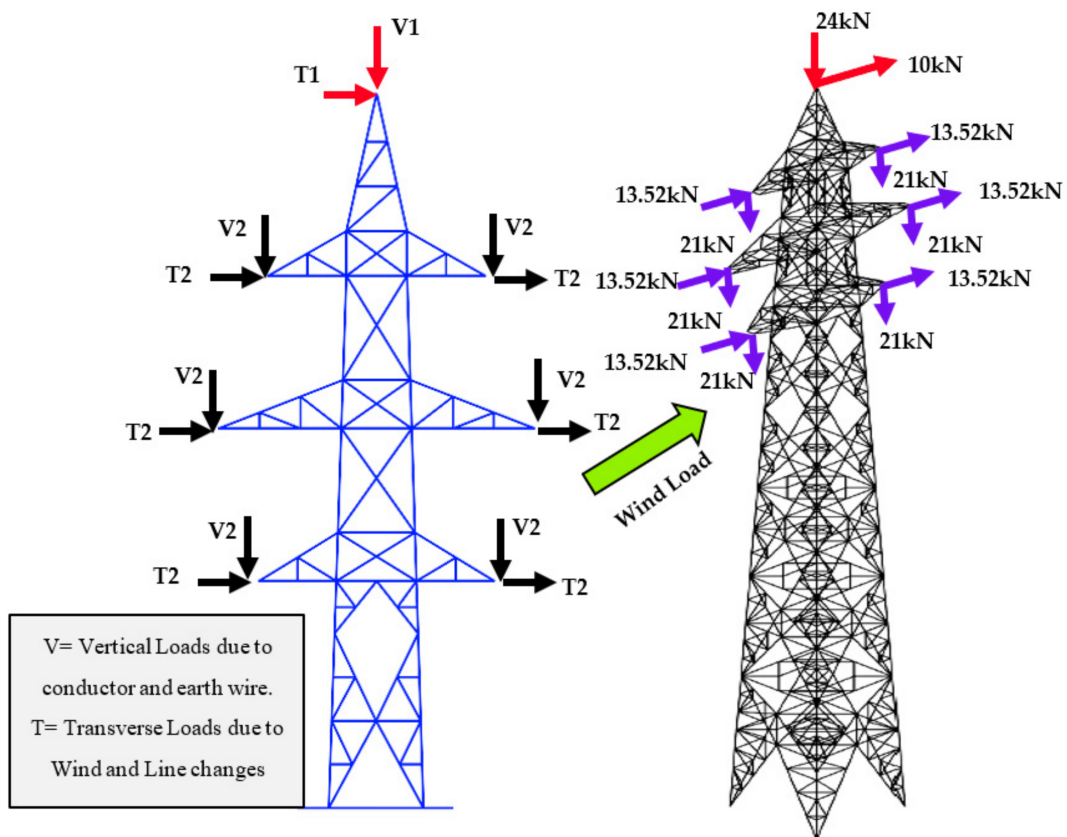


Figure 5. Convention of vertical and transversal structural loading direction.

The dead load is considered as vertical load and consists of the structural weight members, ground wire, and conductor. The dead load of conductor and ground wire acts on the tower cross arm, (V_w) and the top of the tower.

The following equation provides the vertical load of the wire:

$$V_w = wt \text{ of bare wire (kN/m)} + 1.24(d + I)I \times L \times \gamma \tag{1}$$

where,

d referred to diameter of wire in (m)

I denoted to ice thickness (m)

L , designed weight span (m)

γ is the vertical load factor, and equal to 1.50.

The transverse loads are caused by wind pressure on wires and structures, and the transverse component of the line tension at angles. The transverse load due to wind on the wire is given by the following equations:

$$W_h = p \times \frac{d}{12} \times \text{Horizontal Span} \times OCF \tag{2}$$

$$P = 0.6(0.00256)K_zK_{zt}K_dV^2 \tag{3}$$

where,

W_h is the transverse wind load on wire in (kN).

p is the wind pressure in (kN/m²).

d is the diameter on wire in (m).

OCF are the Overload Capacity Factor equals to 2.50.

V is the basic wind speed, 120 mph, and exposure B.

K_z is velocity pressure coefficient, 0.85.

K_{zt} is the topographic factor, 1.0.

K_d is the wind directionality factor, 0.55.

When a line changes direction, the overall transverse load on the structure is equivalent to the sum of the transverse wind load and the transverse component of the wire tension in the new direction. When calculating the total load, the wind direction should be chosen so that the largest resultant load is obtained while considering the impacts on the wires and structure.

The following equation is used to calculate the transverse component of wire tension acting on the structure:

$$H = 2T \sin \theta / 2 \tag{4}$$

where,

H represents the transverse load caused by wire tension in kN

T is the wire tension in kN.

θ is the angle of the line in degrees.

Table 4 describes the basic utilization limits for spotting on the 220 kV transmission line:

Table 4. Basic properties of Tower type A-220 kV, and its vertical and transverse loading on the structure.

Tower Type	A
Utilization	Suspension
Utilization limits	Tangent (0–2°)
Wind span (m)—Max	420
Weight span (m)—Max	850
Weight span (m)—Min	50
Weight/Wind span ratio—Min	0.83 at 0°
Max single span (m)	700
Insulator Weight	70 kg
Ground Wire Load (V1)	24 kN
Transverse Load on Ground Wire (T1)	10 kN
Conductor Wire Load (V2)	21 kN
Transverse Load on Conductor Wire (T2)	13.52 kN

2.3. Non-Linear Dynamic Analysis (NL-DA)

Incremental dynamic analyses were performed by using ground motion data with progressively increasing intensity to the point of collapse. It is also important to record the maximum structural drift, which can be obtained using IDA’s technique. This process is repeated multiple times through dynamically adjusting the seismic loads, step-by-step

(e.g., 0.10, 0.20, 0.30, and so on), until the point of collapse, denoted by Collapse Prevention (CP) state. The IDA curve is derived and established. The IDA curve shows the interaction among both Inter-Storey Drift Ratio (ISDR) as an Engineering Demand Parameter (EDP) and Spectral acceleration $S_a(T_1)$ as an Intensity Measure (IM). The outcomes are compared to the predetermined performance thresholds. According to the FEMA 356, there are three performance levels to estimate tower structural performance, viz., 0.5%, 1.50%, and 2%, corresponding to Immediate Occupancy (IO), Life Safety (LS), and Collapse Prevention (CP), respectively [35]. Following this, the data is used to create the fragility curve.

When the structure becomes unsteady or approaches the collapse limit, the analysis is terminated, since the finite element (FE) platform is used for all visualizations related to the modelling and simulation process. This helps in gaining a comprehensive understanding of the structures' dynamic behaviour. Indeed, it is possible to analyse the anticipated structural response, defects, and monetary loss under earthquakes of varying intensities using IDA. Thus, during seismic excitations, the results of the non-linear time history analysis (NL-THA) are more credible than the results of the non-linear static analysis (NL-SA) for the structural dynamic behaviour.

2.3.1. Intensity Measure

To define earthquake susceptibility and assess earthquake records in the IDAs, scientists use the IM as an indicator to quantify the severity of each event. A structure's vulnerability to ground vibrations can be assessed by considering the quality of the IM. Because the condition of the IM can have a direct impact on the precision and reliability of the PSDM, the selection of the IM is critical in this process. The Peak Ground Acceleration (PGA), Peak Ground Velocity (PGV), spectral acceleration at the fundamental period, $S_a(T_1)$, and Arias Intensity (AI) are a few of the prospective IMs that have been offered by researchers. When comparing various IMs, it has been demonstrated that S_a has a strong correlation with structural demand in the development of PSDMs. Therefore, S_a is employed as the IM in the current study.

2.3.2. Damage Measure

Generally, a Damage Measure (DM) is used to measure the extent of structural seismic damage, and defining it is an essential work in the field of fragility analysis and design. An effective DM is capable of accurately representing the structural dynamic response induced by seismic action excitation. The maximum base shear, peak roof drift, peak floor acceleration, and inter-story drift are the most frequently utilised DMs. Compared to other DMs, the inter-story drift correlates significantly with structural degradation. Inter-Storey Drift Ratio (ISDR), the applicability of which has been demonstrated by Tian et al., is used as the DM in this research.

2.3.3. Limit States

Several limit states known as performance levels are required to accurately depict the structural damage condition during an earthquake in order to be effective. This paper defines three limit states for the transmission tower, as described by [33]. These are: Immediate Occupancy (IO), Life Safety (LS), and Collapse Prevention (CP). The associated ranges of such distinct limit states are considered as 0.5%, 1.50%, and 2.0%, respectively, as previously established [34] and are taken into consideration from FEMA 356. Figure 6 shows the comprehensive mapping relationship between the damage description and the limit states used in this investigation.

2.4. Input Ground Motion Records

When performing nonlinear dynamic analysis, one of the most significant parameters to consider is ground motion selection. Compiling appropriate ground motion records is critical in the process of executing consistent dynamics analysis (NL-DA). For the purposes of this study, and in order to properly account for the limitations of ground motions in

the seismic fragility analysis conducted in this study, a collection of 36 real far-field and near-field seismic data are considered. The 36 strong ground motion records comprised far-field (FF) and near-field (NF) seismic records. These records are evaluated in accordance with the requirements of the basic standards of the international codes, downloaded from the COSMOS database and are shown in Tables 5 and 6.

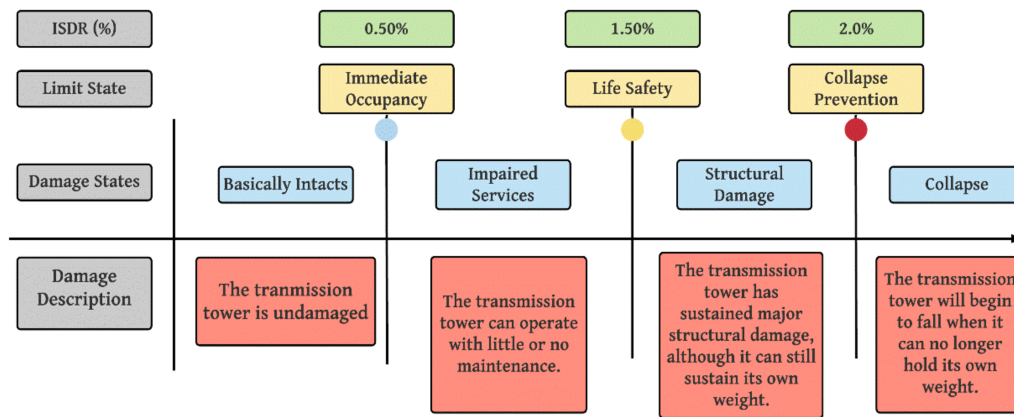


Figure 6. The relationship between the damage description and the limit states.

Table 5. Far-Field ground motion records as an input for nonlinear dynamic analysis.

No.	Earthquake	Year	Station	M _w	PGA(g)	PGV (cm/s)	PGD (cm)	V _{s30} (m/s)
1	Kern County	1952	LA—Hollywood	6.91	0.450	117.79	30.79	308.94
2	Borrego Mtn	1968	El Centro Array #9	6.80	0.499	46.49	42.18	213.44
3	Friuli Italy	1976	Codroipo	5.04	0.554	61.53	7.15	249.28
4	Borrego	1942	El Centro Array #9	6.41	0.277	37.32	4.65	213.44
5	Kern County	1952	LA—Hollywood	6.19	0.446	29.12	9.31	316.46
6	Friuli Italy	1976	Codroipo	5.99	0.368	23.75	17.60	249.28
7	Imperial Valley	1979	Delta	5.61	0.294	65.45	53.12	242.05
8	San Fernando	1976	Buena Vista	6.96	0.486	105.9	93.85	298.68
9	Whittier Narrows-01	1987	Santa Fe Springs	5.99	0.398	23.75	1.76	288.78
10	Loma Prieta	1989	Gilroy Array #	6.74	0.310	64.50	25.65	221.78
11	Sierra Madre	1991	Cogswell Dam	5.61	0.297	15.01	2.050	236.84
12	Kobe	1995	KJMA	6.90	0.854	95.75	24.56	187.77
13	Northridge-0	1994	LA Dam	6.69	0.576	77.09	20.10	184.79
14	Chi-Chi	1999	TCU065	7.62	0.831	129.55	93.85	335.50
15	Morgan Hill	1984	Captiola	6.74	0.444	19.01	4.07	196.42
16	Borah Peak	1983	ETR Reactor Bldg	6.93	0.203	58.27	16.25	214.68
17	San Fernando	1971	Terminal Island	6.21	0.548	40.74	16.01	301.95
18	Imperial Valley	1979	Niland Fire Station	6.80	0.557	82.27	55.05	212.0

Table 6. Near-Field ground motion records as an input for nonlinear dynamic analysis.

No.	Earthquake	Year	Station	M _w	PGA(g)	PGV (cm/s)	PGD (cm)	V _{s30} (m/s)
1	Kern County	1952	Taft Lincoln School	7.40	0.156	15.31	9.21	310.68
2	Tabas, Iran	1978	Ferdows	7.40	0.187	6.53	4.52	302.64
3	Victoria, Mexico	1980	SAHOP Casa Flores	6.30	0.101	7.77	2.45	242.05
4	N. Palm Springs	1986	Hesperia	6.10	0.412	2.32	0.71	198.77
5	Landers	1992	Baker Fire Station	7.30	0.124	17.34	2.28	316.46
6	Northridge-01	1994	Huntington Bch-Waikiki	6.70	0.186	5.01	1.63	184.75
7	Whittier Narrows	1978	Los Angeles, CA	6.10	0.182	63.21	25.36	193.67
8	Imperial Valley	1940	El Centro CA	6.90	0.341	33.14	101.69	213.44
9	Northridge	1994	Sun Valley	6.70	0.457	22.47	51.59	301.95
10	Loma Prieta	1999	Hollister, CA	6.94	0.252	45.14	33.23	221.78
11	Coma Mendocina	1992	Copa Mendocina	7.01	1.400	11.36	95.23	192.05
12	Landers	1992	Lucerne	7.28	0.650	52.29	44.60	208.91
13	Mineral Town	2011	Central Verginia	5.74	0.094	53.64	6.67	219.31
14	Kocaeli	1999	Sakarya	7.40	0.230	55.83	184.60	249.28
15	Chi Chi	1999	TCU102	7.60	0.390	65.48	193.30	335.50
16	Coyote lake	1979	Gilroy Array	5.74	0.333	27.14	4.48	202.85
17	Morgan hill	1984	Anderson Dam	6.19	0.276	29.52	6.44	192.26
18	Nahanni, Canada	1985	Site1	6.76	1.170	36.53	4.66	317.45

In this study, the 32 seismic records considered are characterised as having site class D within the Magnitude (M_w) ranges of 5.0 to 8.0, and are categorised as Far-Field (FF) records with Epi-central Distance more than 20 km and Near-Field (NF) records with Epi-central Distance less than 20 km. Since a majority of the structures are installed on soft soil in Lebanon with features corresponding with soil type D, this is an appropriate classification. Moreover, the classification track from the site to the source for the far-field and near-field records is not completely stated, but the source-distance relationship associated with the natural frequency has a significant impact on the near-field in which the structure is located. However, according to FEMA P695, far-field records are determined whenever the distance between stations surpasses or is equal to 10 kilometres from the geological fault movement, but near-field records are described when the distance between stations is less than 10 kilometres from the split fault. There is no universally accepted rationale for a location to be classified as near or far-field.

Several criteria recommended by [36–41], such as magnitude (M_w), Peak Ground Acceleration (PGA), and distance from the source should be considered when choosing ground motions. These include the near-field (<20 km) and far-field (>20 km) limits, as well as the soil type. To fully comprehend these aspects, a spectrum of PGA is examined. A full-range of the PGA record values is used, and all the records fall in the range of 0.09 g to 1.40 g with a mean of 0.386 g in the case of far-field records. The average PGA is 0.466 g with a range of 0.20 g to 0.86 g for near-field seismic scenarios. Subsequently, the chosen ground motion datasets for two seismic scenarios (FF and NF) are normalised or scaled by utilising the Seismomatch program, according to the Lebanese seismic standard targeted by its response spectrum as shown in Figures 7 and 8. Here, $Z = 0.25$ g, $C_a = 0.32$, $C_v = 0.47$ according to UBC97 corresponding to Lebanese seismic norm, and with $S_1 = 0.4$, and $S_1 = 1.20$, taking into account site coefficient ($F_a = 1.0$) and ($F_v = 1.6$) for site class D by referring to 2009 IBC MCE spectral response acceleration.

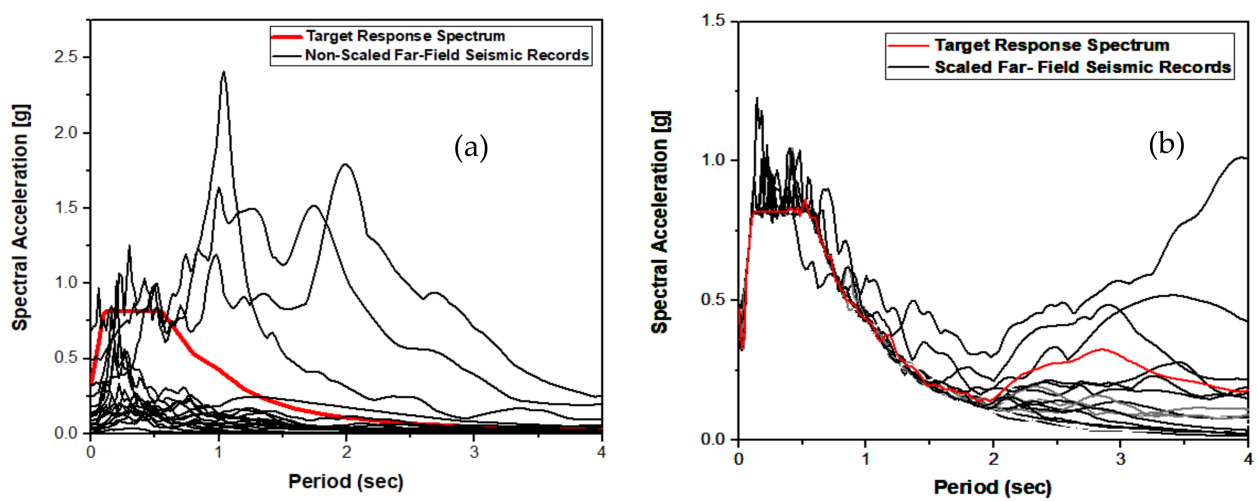


Figure 7. Far-field ground motion seismic records (a): Before matching with target spectrum, (b) After matching with target spectrum.

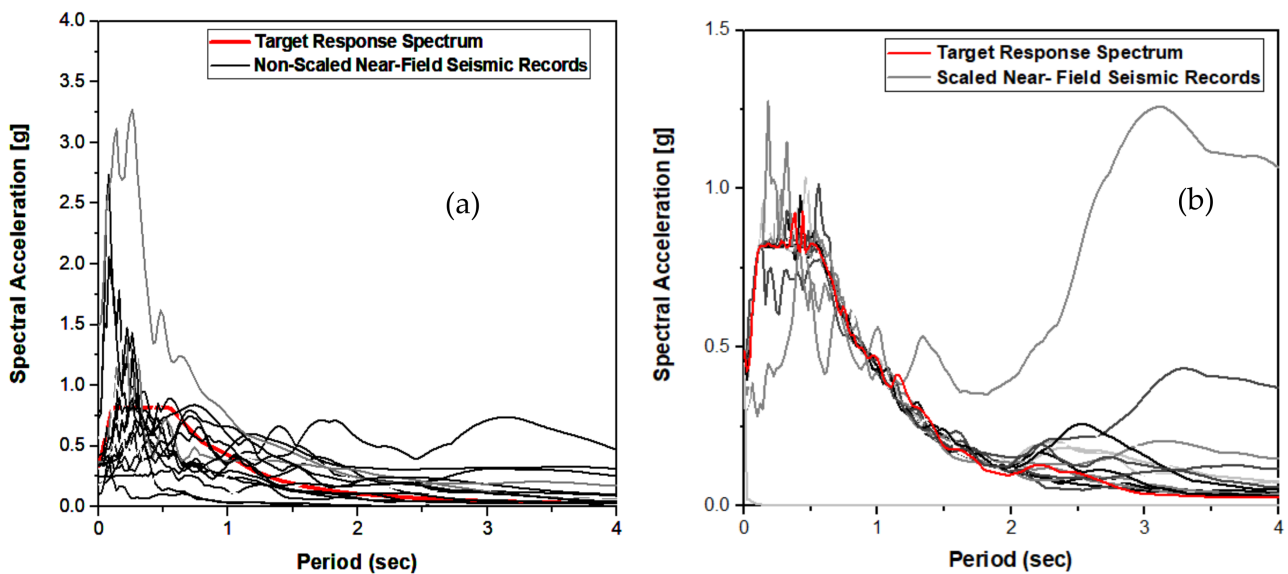


Figure 8. Near-field ground motion seismic records (a): Before matching with target spectrum, (b) After matching with target spectrum.

Due to the scarcity of true repeated earthquake data, this study relies solely on artificial sequences to simulate earthquake activity. Hatzigeorgiou and Liolios [42], as well as other researchers, such as Zahid, et al. [43], Fazli and Majid [44], and Faisal, et al. [45], have earlier adopted the method that can be scaled up to produce a series earthquake, as shown in the diagram below.

Every ground motion record is assigned two true seismic sequences. Each single ground motion record for each event has a time interval of 15 s between them. A gap time delay of 100 s is placed between the two successive earthquake incidents to compensate for the timing difference. Hatzigeorgiou and Liolios [42] proposed the time gap, and it is sufficient to restore the structure to its rest state after being shaken. Using the Pacific Earthquake Engineering Research Center (PEER) database, three repeating incidents are picked in this study. The selected range of magnitude (M_w) is 5–7 Richter scales. The PGA intensity measure is taken between 0.113 g and 0.447 g, as illustrated in Figure 9.

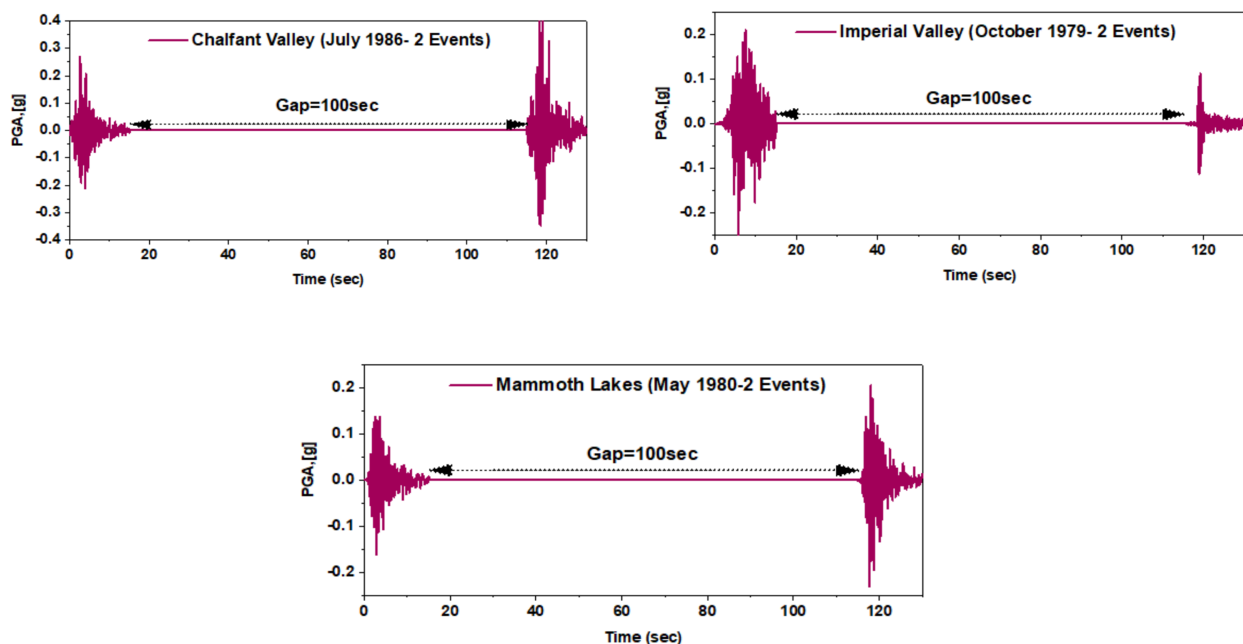


Figure 9. Selection of repeated ground motion successive seismic events.

2.5. Probabilistic Distribution Function Using Fragility Curve

Kennedy, et al. [46] proposed the concept of seismic fragility analysis to evaluate the probabilistic seismic performance of a nuclear power station, and it has since evolved into a sophisticated analytical tool for analysing the seismic risk of various structures. With a particular intensity measure of ground motions, seismic fragility is defined as the conditional probability of attaining or exceeding a specified damage state. Fragility assessment is a technique of estimating the risk of a seismic event on a structural model, and it is a useful method for estimating the likelihood of structural damage. For far-field and near-field ground movements, the fragility curve represents the probability of collapse with regard to the IM. Along with the ISDR, it is used as a damage measure to detect serious deterioration that could lead to structural collapse under seismic scenarios.

In seismic risk assessment, fragility functions are powerful statistical tools that can be used to understand the dynamic response of transmission towers. They are the link between a given seismic IM and the likelihood of reaching or exceeding a specific damage state. In this study, $S_a(T1)$ is used as the seismic IM to develop the fragility curves. There are two processes involved in the formation of the fragility curves. The mean and standard deviation of the collapse capacity is computed at the initial stage. The second stage involves the development of the fragility curve from the obtained values of mean and standard deviation using the lognormal Cumulative Distribution Function (CDF).

Since $Sa(T1)$ is used in this work as the seismic IM for the IDA, the same parameter is also employed in the development of the fragility curves. Suppose the fragility curve is being drawn for the Collapse Prevention (CP) state. The $Sa(T1)$ values that lead to the collapse state recorded from IDA would be used in the calculation of the fragility curve. In this work, a variety of $Sa(T1)$ values are recorded under a variety of various ground motion records. Then, the mean and standard deviation of these values are calculated and used in Equations (1) and (2). Using the established fragility curves for all permutations of the transmission tower, the seismic performances of the structural models are evaluated in terms of IO, LS, and CP performance limit states.

$$P[\text{Damage}/Sa(T1)] = \phi\left(\frac{\ln(Sa[T1]) - (\mu)}{\sigma}\right) \quad (5)$$

where ϕ is the standard normal cumulative distribution function, μ and σ are the mean and standard deviation of logarithm $Sa(T1)$.

2.6. Collapse Margin Ratio

Since its inception in FEMA P695, the Collapse Margin Ratio (CMR) has been commonly considered as one of the most accurate seismic indicators of a structure's collapse safety. It is defined by the Federal Emergency Management Agency (FEMA) as the proportion of median collapse intensity determined from a fragility curve to intensity of the Maximum Considered Earthquake (MCE) ground motion. Structure stability and collapse proneness are two important parameters in seismic evaluation that must be considered. It is a crucial metric in seismic evaluation since it describes structural stability and collapse risk.

According to the Lebanese seismic norm, the PGA is associated with a 10% probability of exceedance in 50 years. The collapse probability due to the MCE ground motions is limited to 10% according to the FEMA P695 (FEMA, 2009). As a result, the PGA in Lebanon associated with the 10% probability of exceedance in 50 years remains unchanged. CMR is defined as the ratio of ground motion intensity corresponding to the 50% probability of structural collapse to the ground motion intensity corresponding to the design MCE level, as shown in Equation (6).

$$\text{CMR} = \frac{IM_{50\% \text{ collapse}}}{IM_{\text{MCE}}} \quad (6)$$

where $IM_{50\%}$ is the ground motion intensity corresponding to the 50% probability of structural collapse; I_{MCE} is the ground motion intensity corresponding to the MCE level for the design. The MCE intensity used is 0.25 g according to the Lebanese seismic hazard map. Figure 10 shows the framework of the seismic vulnerability assessment for the transmission tower under the effect of three seismic scenarios.

2.7. Structural Dynamic Properties

Modal analysis is performed in this study to better understand and identify the dynamic behaviour of a mechanical structure. Modal analysis is the determination of natural frequencies, mode shapes and modal damping of a system using Frequency Response Function (FRF) measurements. However, the study will focus on the mode shapes and natural frequencies of the telecommunication steel tower. This is because the mode shapes and natural frequencies of any mechanical system are likely the single most essential attribute. As a result, the designer can well understand all the forms of vibrations that are feasible by knowing each mode shape of the structure.

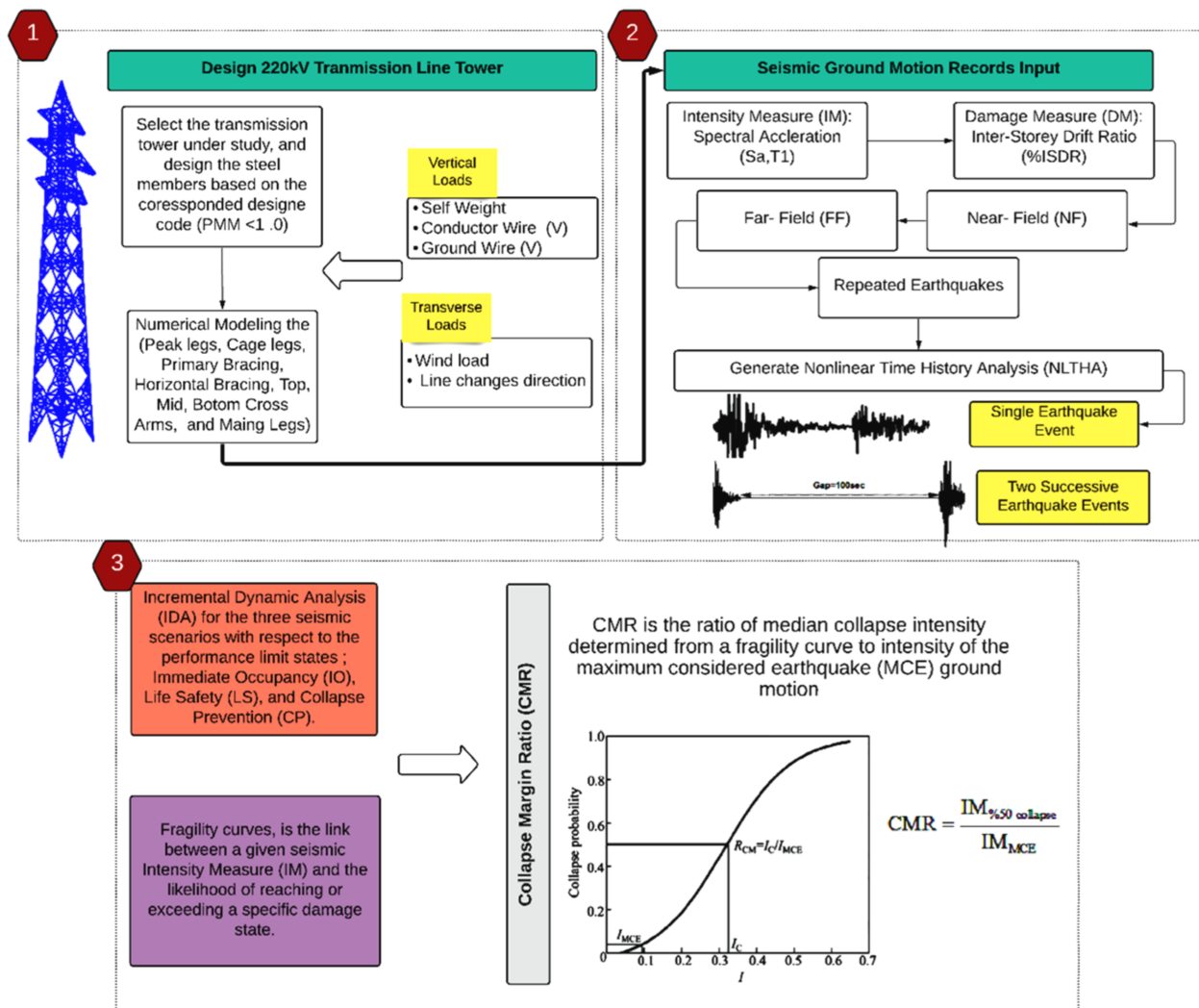


Figure 10. Transmission tower assessment under the effect of three seismic scenarios ((1) far-field, (2) near-field, and (3) repeated earthquakes).

Mode shape is defined as the structure deforming or vibrating in a given shape when it is excited at a particular natural frequency. The transmission steel tower has many mode shapes, which means that each mode shape has its own natural frequency. In any case, the first three modes of the tower will be discussed. The first three mode shapes of the tower are shown in Figure 11 and the natural frequency for the first three mode shape is shown in Table 7. The tower is excited at its first frequency with 0.942 Hz, it deforms and translates along the Y-axis as shown in Figure 11a. The second mode shape of the tower, as shown in Figure 11b, translate along X-axis at 1.267 Hz. The tower is excited at the third frequency with 1.536 Hz, and the third mode shape is on contrary with the first two mode shape, which is rotated about the Z-axis as shown in Figure 11c. The natural frequency of the tower increases as the mode number increases from the observation. The result also demonstrates that as the number of modes increases, so will the node points.

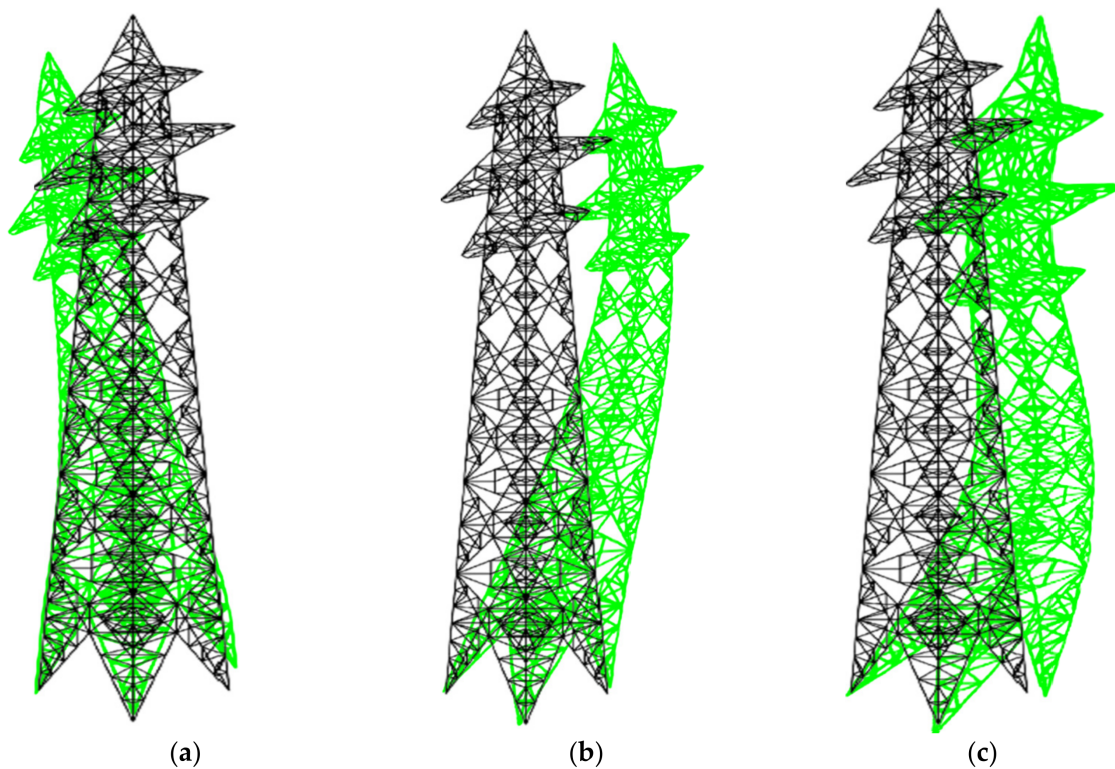


Figure 11. Mode shape for transmission steel tower, (a): 1st Mode shape, (b): 2nd Mode shape, and (c): 3rd Mode shape.

Table 7. Natural Period and frequency of the first three mode deforming shapes.

Number of Mode	Natural Period (s)	Natural Frequency (Hz)	Deformed Shape
1	1.061	0.942	Translating in Y-axis (Longitudinal)
2	0.789	1.267	Translating in X-axis (Transversal)
3	0.651	1.536	Rotating about Z-axis (Torsion)

The natural frequency of the tower should never coincide with the excitation frequency. This is to avoid the tower from exhibiting extremely high amplitude vibrations, which could cause the tower to collapse and fail if the excitation frequency coincides with a natural frequency of the tower. The tower can be redesigned or modified to move the natural frequency of the tower away from the excitation frequency to avoid this issue, for example, by enhancing the stiffness of the frame members. As a result, making sure that the tower's natural frequencies must be greater than any excitation frequency.

3. Results and Discussion

3.1. Incremental Dynamic Analysis (IDA)

It is critical to understand the structural performance of transmission steel tower line systems during a variety of ground motions. Incremental dynamic analysis is a quantitative technique that is used to evaluate the important elements that control structural performance and its seismic capacity based on the performance limit states provided by FEMA 356 and recommended by the Performance-Based Earthquake Engineering (PBEE) framework. In this reported work, a simulation of Strong Ground Motions (SGM) is carried out to predict the seismic performance of a structure utilising an array and variety of

ground motion records relating to far-field earthquakes as well as near-field and repetitive earthquakes. The IDA curves are plotted with the IM of the $Sa(T1, g)$ against the EDP of the ISDR in order to provide an overview of the seismic performance of the tower under three seismic scenarios (far-field, near-field, and repetitive) ground motions until collapse point is reached as shown in Figure 12.

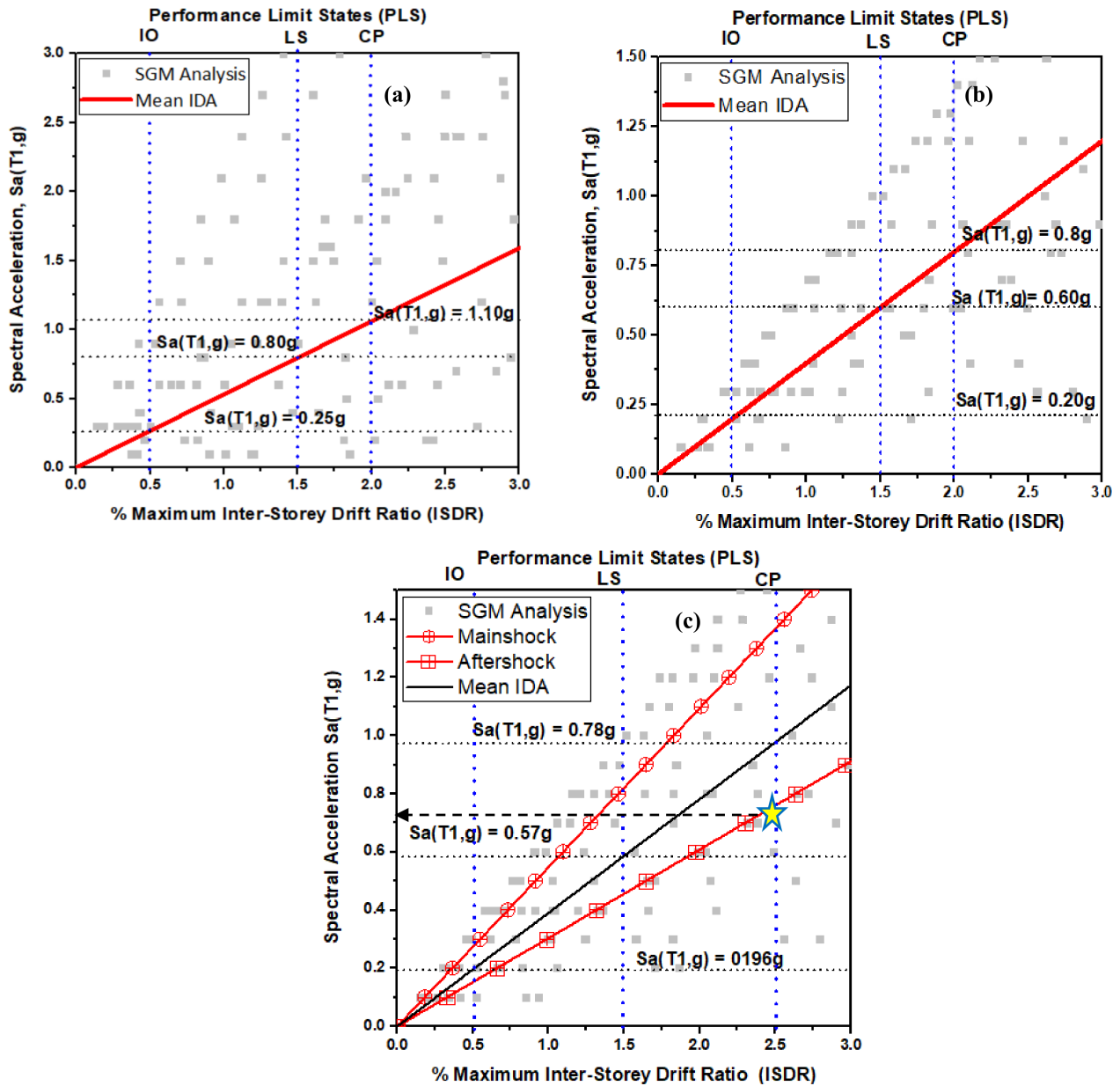


Figure 12. IDA curves for three seismic scenarios; (a): Far-Field, (b): Near-Field, and (c): Repetitive earthquakes.

The overall seismic capability performance towards the tower is similar for the three seismic scenarios at the IO performance level, implying that the tower retains much of its original strength and stiffness. This, in turn, means that the tower is in continuous service with negligible tower damage. There may be minor cracking in the structural frame elements of the tower. The far-field ground motion requires 0.25 g while near-field and repetitive ground motions require 0.20 g and 0.196 g, respectively, to reach the IO performance level. Furthermore, in order to achieve the LS performance level, the far-field, near-field, and repetitive ground motions required 0.80 g, 0.60 g, and 0.57 g as the mean of

mainshock and aftershock, respectively. In this level, the tower sustains severe damage, but there is still some safety from a catastrophic tower collapse, resulting in moderate overall damage. A certain amount of residual strength and stiffness continue to remain in all tower levels, causing serious damage to a few tower frame components, although this may not create substantial falling debris risks, either inside or outside the tower. Moreover, at the CP performance level, the far-field, near-field, and repetitive seismic scenarios require 1.10 g, 0.80 g, and 0.78 g, respectively. The tower is at the point of total collapse due to considerable degradation in the strength and stiffness of the lateral-force-resisting system and massive permanent lateral deformation of the structure. As a result, it's possible that the tower may not be repairable and may not be safe to rebuild. The tower may fall if an aftershock occurs that results in a CP state at spectral acceleration 0.71 g with a 50% difference with the mainshock that was achieved the CP state at 1.41 g. This shows that repetitive earthquakes are more damaging to the structure compared to single earthquakes in both far-field and near-field; the far-field attains CP damage state at 1.10 g, and the near-field at 0.80 g, which the aftershock reaches earlier at 0.71 g. However, in the case of far-field ground motions, the transmission tower has better performance than for near-field ground motions, with a mean difference of 27.3% between the two ground motions.

The findings for single seismic events show that the near-field ground motion is more destructive than far-field ground motion as aforementioned by some researchers [29,47]. Similarly, repetitive earthquakes are more damaging and intense than both seismic scenarios related to far-field and near-field. This can be shown by the fact that the gradient of the mean of line in far-field ground motion is lower than the near-field ground motion. This indicates that the tower frame components would be more severely damaged if they are under near-field and repetitive ground motion excitations. For more clarification, Figure 13 shows the buckling, compression, and tensile failure during the three seismic scenarios at the life safety stage, considering it as a repairable stage.

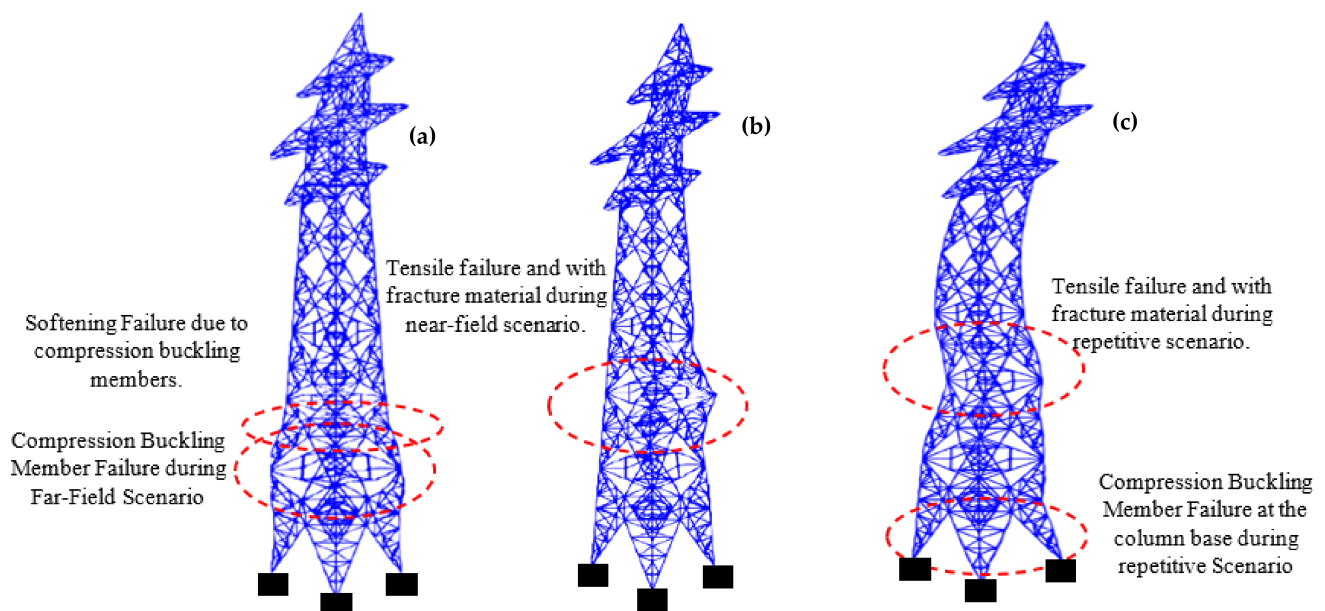


Figure 13. Deformation and failure mode for three seismic scenarios at life safety/repairable stage; (a): Far-Field, (b): Near-Field, and (c): Repetitive earthquakes.

3.2. Fragility and CMR Analysis

The seismic performances of the transmission steel tower under Far-Field (FF), Near-Field (NF) and Repeated ground motion records were determined using fragility curves by recording the damage for three performance limit states (IO, LS, and CP) in terms of possibilities of damages at two different intensities of spectral acceleration $S_a(T1, g)$, which

were chosen at 1.0 g and exceeding 1.0 g for observing the dynamic behavior of the selected tower as shown in Figure 14.

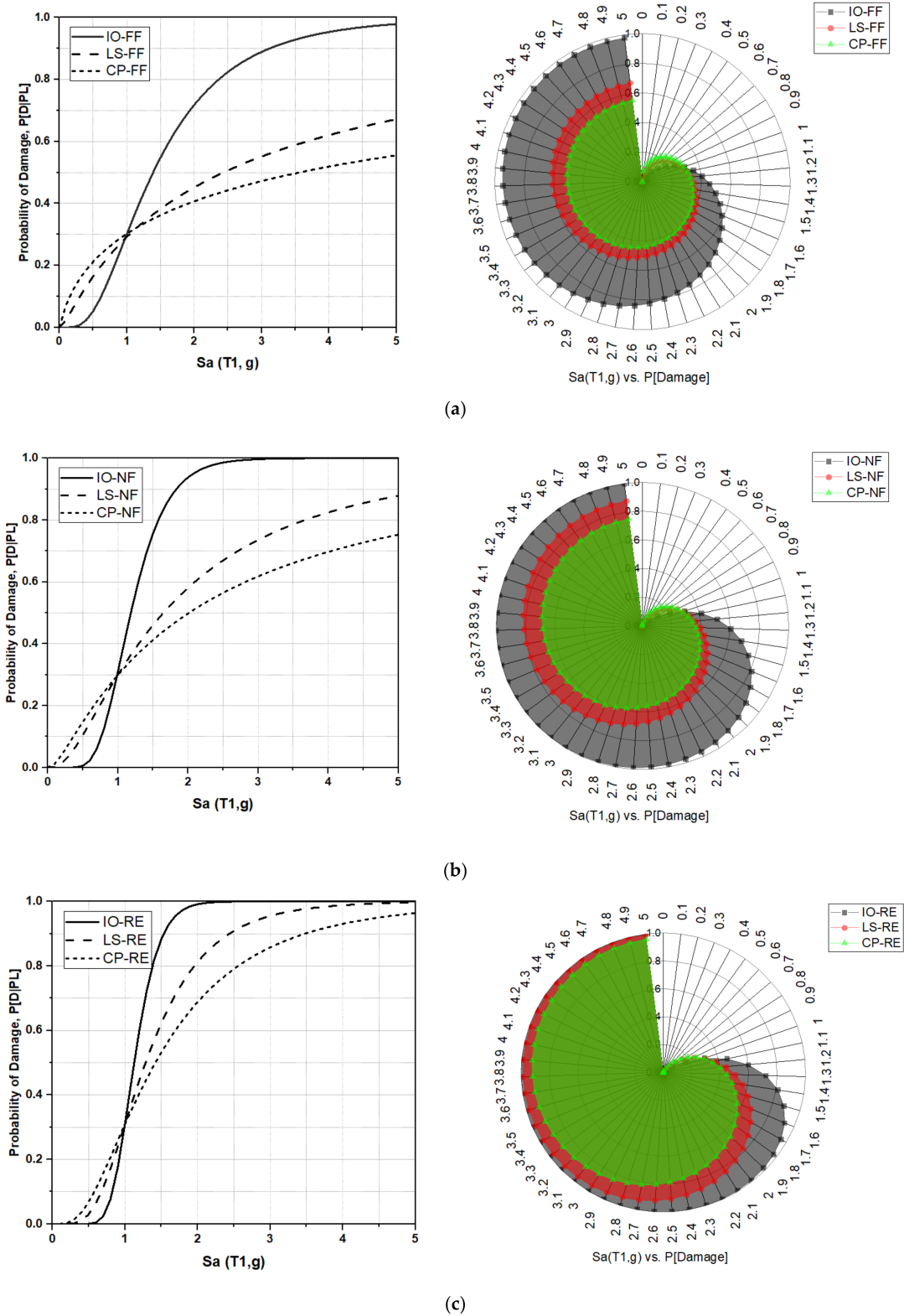


Figure 14. Fragility curves for three seismic scenarios based on the relation between Sa(T₁, g) and P[Damage]; (a): Far-Field, (b): Near-Field, and (c): Repetitive earthquakes.

At intensity measure 1.0 g, the three performance levels, IO, LS and CP, for the three seismic scenarios intersect at the $S_a(T1, g) = 1.0$ g, having the same possibility of damage which roughly equals 30%. Nevertheless, before reaching the inflection point of 1.0 g, the probabilities of damage in the case of far-field seismic scenarios for the three performance levels are substantially greater than the near-field and repeated seismic scenarios. However, beyond 1.0 g as the inflection point in this study, the probabilities of damage for the three performance levels at the far-field ground motion become significantly lower than the near-field and repetitive ground motions. For example, at intensity measure 2.0 g, the possibilities of damage for reaching or exceeding the IO state are 70%, 90%, and 100% for far-field, near-field, and repeated ground motions, respectively. However, at the same intensity measure, the structure showed the possibility of damages during far-field 45%, and 40, for LS and CP states, respectively. The possibility of damage becomes more significant when near-field ground motion has impacted the tower by reaching (60%, and 50%), and during repetitive events 80%, and 70% for LS and CP states, respectively.

The occupancies of structures are considered to be critical and must be monitored during earthquake events. When considering near-field ground motions and multiple scenarios, it can be seen that the structures rapidly lose their occupancies as the intensity measures increase; in the case of near-field, the structure possibility of damage to be complete in-occupant of 100% occurring at 2.50 g, which vanishes earlier compared to the far-field events that achieved this stage at 5.0 g, and earlier at 2.0 g during repetitive ground motions, which is clearly showing in the radar graph between S_a and probability of damage as shown in Figure 14.

Furthermore, a structure's life safety is threatened during seismic events, and it is considered an important stage after the structure occupancy stage that could help in estimating the need for repair. In this study, the three seismic scenarios have different life safety states. However, considering the 50% possibility of damage as half-life threatening structures is the key for monitoring the tower structural behaviour. Starting with the far-field seismic events, the structure can be retrofitted if the intensity measure does not exceed the 2.50 g spectral acceleration. On the other hand, during near-field seismic events, the structures can be repaired if the intensity measure equals 1.50 or less, and 1.20 g in case of multiple seismic scenarios.

According to the collapse margin ratio (CMR) initially proposed by FEMA P695, the intensity measure ($I_{50\%}$) for reaching 50% of the structural collapse for the far-field, near-field and repeated earthquakes are 3.50 g, 2.0 g, and 1.40 g, respectively. From these values and the Maximum Considered Earthquake (MCE) value of 0.30 related to the Lebanese seismic hazard map, the CMR is established. For the far-field seismic scenario, the CMR equals 11.67, whereas, for near-field excitations, the CMR value drops to 6.67, which is 50% less safe than the far-field events. However, for repetitive earthquakes, the CMR score is 4.67 which is more significant to obtain more vulnerable detections on the structures. As a result, the collapse rate of the tower under far-field ground motion excitation is lower than for the near-field and repetitive ground motion cases, since the CMR of the far-field ground motion shows the highest value. Thus, the use of CMR as a seismic measure can be useful for the evaluation of the tower during seismic events.

The outcomes from the IDA and fragility analysis are consistent with the CMR. Furthermore, the analyses demonstrate that the transmission steel tower under near-field ground motion excitation is more likely to collapse than a tower under far-field ground motion excitation during a single event, and more likely to damage under multiple seismic events, showing that the tower can withstand the desired seismic performance or MCE of 0.30 g in keeping with the Lebanese seismic norm. Figure 15 shows the fragility curve related to CMR values and their intensity measures and Table 8 shows the CMR values obtained from the fragility curves.

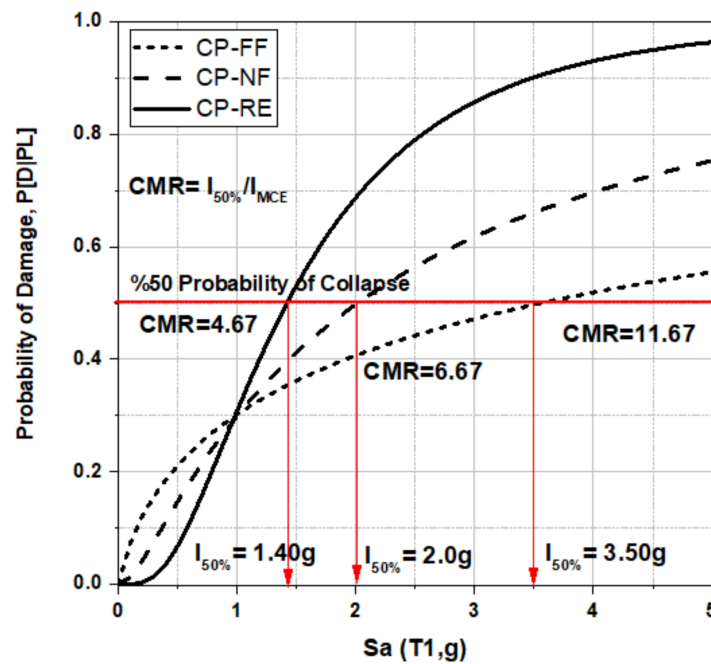


Figure 15. Collapse fragility curves, far-field, near-field, and repetitive earthquakes.

Table 8. CMR values for three seismic scenarios.

Seismic Scenarios	I_{MCE} (g)	$I_{50\%}$ (g)	CMR
Far-Field	0.30	3.5	11.67
Near-Field	0.30	2.0	6.67
Repeated Earthquakes	0.30	1.4	4.67

Finally, the results show that the frame elements of the transmission steel tower would suffer significant damages under near-field and repetitive ground motion than far-field ground motion, despite the fact that the damage probability at far-field ground motion is greater than near-field ground motion before achieving 1.0 g. As a result, the tower damages caused by near-field ground motion as a single event and repetitive ground motions as multiple events are extremely devastating, as the damage probabilities for the three performance levels are much higher than the far-field ground motion.

4. Conclusions

This paper uses the probabilistic seismic demand model to investigate the seismic vulnerability of transmission towers in terms of the maximum Inter-Storey Drift Ratio (ISDR) and the intensity measure related to spectral acceleration. Incremental dynamic analysis is performed to estimate the capacity limit state for the transmission tower, and the IDAs are utilised to obtain the fragility functions and the Collapse Margin Ratio (CMR). Finally, three seismic scenarios (Far-Field, Near-Field, and Repeated Earthquakes) are used to estimate the tower seismic performance of multi-component seismic excitations using NL-THA. Based on the results, the following significant conclusions are drawn:

- (1) For the failure mechanism for the structures, the deformation and failure mode for far-field is buckling failure in its frame members. For the near-field case, it is tensile failure with fracture material, which becomes worse when subjected to repetitive aftershock excitation that results in a combination of tensile failure with material fracture and compression buckling at the base of the columns.
- (2) From the IDA curves, for both far-field and near-field, repetitive earthquakes are more damaging to the structure than single events; the far-field case results in CP damage state at 1.10 g and the near-field at 0.80 g, while aftershock results in CP damage state

at 0.71 g. However, the transmission tower performs far better in the case of far-field ground motions than near-field. It can be concluded that the frame elements of the transmission steel tower suffer significant damages under near-field and repetitive ground motion than under far-field ground motion, despite the fact that the damage probability at far-field ground motion is greater than near-field ground motion before achieving 1.0 g.

- (3) From the fragility curves, the occupancy and life safety limit states are considered crucial in monitoring the seismic performance for the possibility of capacity recovery post seismic events. The structure rapidly loses occupancy during near-field and repetitive seismic events and is more life threatening compared to far-field excitations. As long as the intensity does not exceed 2.50 g, the structure can be repaired. When structures are subjected to near-field seismic occurrences, the structures can benefit from repair attempts if the intensity measure is 1.50 or less, and 1.20 g or less in the case of several seismic scenarios. The radar view provides a clear view of the difference between the three seismic scenarios.
- (4) From CMR, the rate of collapse for the transmission steel tower is lower under far-field ground motion than under near-field and repetitive ground motions. This is because the CMR for the far-field ground motion is greater than that of the near-field ground motion; the CMR values are 11.67, 6.67, and 4.67 for the far-field, near-field, repetitive ground motions, respectively. When considered as a single event, the analyses show that the transmission steel tower is more likely to collapse than a tower under far-field ground motion excitation and that the tower is more likely to damage during multiple seismic events, demonstrating that the tower can withstand the desired seismic performance or MCE of 0.30 g according to the Lebanese seismic norm. This verifies the accuracy of the results of the IDA and fragility analyses.

This work shows the existence of research opportunities to determine the limit states through incremental dynamic analysis and fragility curves. This method is expected to be accurate since the high-order modes of the transmission tower can be considered for three seismic scenarios that are necessary to be incorporated in the earthquake engineering field which usually ignored the effect of seismic forces on the structures to be designed for wind forces.

Author Contributions: Conceptualization and Methodology: M.M.K. and F.M.N.; investigation, M.M.K., W.Q.M. and C.G.T.; writing—original draft preparation, M.M.K. and C.G.T.; writing—review and editing, M.M.K., W.Q.M. and F.M.N.; visualization, F.M.N. and S.B.; supervision, F.M.N. and S.B. All authors have read and agreed to the published version of the manuscript.

Funding: This research was funded by Internal Research Grant OPEX, grant type “J510050002-IC-6 BOLDREFRESH2025-CENTRE OF EXCELLENCE”.

Institutional Review Board Statement: Not Applicable.

Informed Consent Statement: Not Applicable.

Data Availability Statement: Data sharing is not applicable to this article.

Acknowledgments: The authors acknowledge Universiti Tenaga Nasional, Malaysia (J510050002-IC-6 BOLDREFRESH2025-CENTER OF EXCELLENCE) for the financial supports for this study.

Conflicts of Interest: The authors declare no conflict of interest.

References

1. Pan, H.; Li, C.; Tian, L. Seismic fragility analysis of transmission towers considering effects of soil-structure interaction and depth-varying ground motion inputs. *Bull. Earthq. Eng.* **2021**, *19*, 4311–4337. [[CrossRef](#)]
2. Pan, H.; Tian, L.; Fu, X.; Li, H. Sensitivities of the seismic response and fragility estimate of a transmission tower to structural and ground motion uncertainties. *J. Constr. Steel Res.* **2020**, *167*, 105941. [[CrossRef](#)]
3. Holmes, W.; Sommers, P. Northridge Earthquake Reconnaissance Report, Vol. 2. *Earthq. Spectra* **1996**, *11*, 125–176.
4. Shinozuka, M. *The Hanshin-Awaji Earthquake of January 17, 1995 Performance of Lifelines*; Technical Report; National Center for Earthquake Engineering Research (NCEER): Buffalo, NY, USA, 1995; p. 225.

5. NCREE. *Investigation Report of Chi-Chi Earthquake*; National Center for Research on Earthquake Engineering: Taipei, China, 1999.
6. Yu, Y.; Li, G.; Li, P.; Zhu, Q.; Yuan, D.; Wang, C.; Li, J.; Huang, H.; Li, L.; Zhang, X. Investigation and analysis of electric equipment damage in Sichuan power grid caused by Wenchuan earthquake. *Power Syst. Technol.* **2008**, *32*, 1–6.
7. Zhang, D.; Zhao, W.; Liu, M. Analysis on seismic disaster damage cases and their causes of electric power equipment in 5-12 Wenchuan earthquake. *J. Nanjing Univ. Technol.* **2009**, *31*, 345–407.
8. Khedr, M.A.; McClure, G. A simplified method for seismic analysis of lattice telecommunication towers. *Can. J. Civ. Eng.* **2000**, *27*, 533–542. [[CrossRef](#)]
9. Aghaeipoor, M.; Alembagheri, M. Seismic Damage of Submerged Intake Tower under the Sequence of Mainshocks and Aftershocks. *J. Earthq. Eng.* **2021**, 1–25. [[CrossRef](#)]
10. Raj, S.V.; Kumar, M.; Bhatia, U. Fragility curves for power transmission towers in Odisha, India, based on observed damage during 2019 Cyclone Fani. *arXiv* **2021**, arXiv:2107.06072.
11. Saini, D.K.; Sharma, M. Techno-economic hardening strategies to enhance distribution system resilience against earthquake. *Reliab. Eng. Syst. Saf.* **2021**, *213*, 107682.
12. Azeem, M.; Aliya, I. Approximation of seismic plication effects on rooftop telecommunication towers. *Int. J. Civ. Eng.* **2018**, *9*, 620–634.
13. El-Zayyat, H.M.; El-Isa, Z.H.; El-Tayem, A.A.; Abdel-Fattah, B.A. Seismic Evaluation of The Towards of Aqaba-Amman 400 KV Overhead Transmission Line.(Dept. E). *MEJ Mansoura Eng. J.* **2021**, *17*, 24–41. [[CrossRef](#)]
14. Zhao, B.; Wu, D.; Lu, Z. Shaking table test and numerical simulation of the vibration control performance of a tuned mass damper on a transmission tower. *Struct. Infrastruct. Eng.* **2021**, *17*, 1110–1124. [[CrossRef](#)]
15. Barrera, J.; Beaupuits, P.; Moreno, E.; Moreno, R.; Muñoz, F.D. Planning resilient networks against natural hazards: Understanding the importance of correlated failures and the value of flexible transmission assets. *Electr. Power Syst. Res.* **2021**, *197*, 107280. [[CrossRef](#)]
16. Lorenzo, I.F.; Elena, B.C.; Rodríguez, P.M.; Parnás, V.B.E. Dynamic analysis of self-supported tower under hurricane wind conditions. *J. Wind. Eng. Ind. Aerodyn.* **2020**, *197*, 104078. [[CrossRef](#)]
17. Rezayibana, B. The Effect of Soil Type on Seismic Response of Tall Telecommunication Towers with Random Vibration Analysis. *Int. J. Eng.* **2020**, *33*, 419–426.
18. Tsavdaridis, K.D.; Nicolaou, A.; Mistry, A.D.; Efthymiou, E. Topology optimisation of lattice telecommunication tower and performance-based design considering wind and ice loads. In *Structures*; Elsevier: Amsterdam, The Netherlands, 2020; Volume 27, pp. 2379–2399.
19. Chandra, T.; Sengupta, S. Dynamic Analysis of Telecommunication Tower for Optimum Modal Combination and Elemental Discretization. *Int. J. Eng. Adv. Technol.* **2019**, *9*, 2229–2237. [[CrossRef](#)]
20. Szafran, J.; Juszczak, K.; Kamiński, M. Experiment-based reliability analysis of structural joints in a steel lattice tower. *J. Constr. Steel Res.* **2019**, *154*, 278–292. [[CrossRef](#)]
21. Chen, B.; Guo, W.; Li, P.; Xie, W. Dynamic responses and vibration control of the transmission tower-line system: A state-of-the-art review. *Sci. World J.* **2014**, *2014*, 1–20. [[CrossRef](#)]
22. Chen, B.; Weng, S.; Zhi, L.; Li, D. Response control of a large transmission tower-line system under seismic excitations using friction dampers. *Adv. Struct. Eng.* **2017**, *20*, 1155–1173. [[CrossRef](#)]
23. Assi, R. *Seismic Analysis of Telecommunication Towers Mounted on Building Rooftops*; McGill University: Montreal, QC, Canada, 2006; Volume 68.
24. Albayrak, U.; Morshid, L. Evaluation of seismic performance of steel lattice transmission towers. *Civ. Eng. J.* **2020**, *6*, 2024–2044. [[CrossRef](#)]
25. Kassem, M.M.; Nazri, F.M.; Farsangi, E.N. On the quantification of collapse margin of a retrofitted university building in Beirut using a probabilistic approach. *Eng. Sci. Technol. Int. J.* **2020**, *23*, 373–381. [[CrossRef](#)]
26. Kircher, C.; Deierlein, G.; Hooper, J.; Krawinkler, H.; Mahin, S.; Shing, B.; Wallace, J. *Evaluation of the FEMA P-695 Methodology for Quantification of Building Seismic Performance Factors*; National Institute of Standards and Technology: Gaithersburg, MD, USA, 2010; pp. 1–421.
27. Patil, A.; Jung, S.; Kwon, O.-S. Structural performance of a parked wind turbine tower subjected to strong ground motions. *Eng. Struct.* **2016**, *120*, 92–102. [[CrossRef](#)]
28. Heydari, M.; Mousavi, M. The comparison of seismic effects of near-field and far-field earthquakes on relative displacement of seven-storey concrete building with shear wall. *Curr. World Environ.* **2015**, *10*, 40. [[CrossRef](#)]
29. Tian, L.; Pan, H.; Ma, R.; Qiu, C. Collapse simulations of a long span transmission tower-line system subjected to near-fault ground motions. *Earthq. Struct.* **2017**, *13*, 211–220.
30. Long, X.; Wang, W.; Fan, J. Collapse analysis of transmission tower subjected to earthquake ground motion. *Model. Simul. Eng.* **2018**, *2018*. [[CrossRef](#)]
31. Huijter, C.; Harajli, M.; Sadek, S. Re-evaluation and updating of the seismic hazard of Lebanon. *J. Seismol.* **2016**, *20*, 233–250. [[CrossRef](#)]
32. Huijter, C.; Harajli, M.; Sadek, S. Upgrading the seismic hazard of Lebanon in light of the recent discovery of the offshore thrust fault system. *Leban. Sci. J.* **2011**, *12*, 67.
33. ASTM. *Guide for Design of Steel Transmission Towers*; American Society of Civil Engineers: New York, NY, USA, 1971.

34. Farr, H.H. *Transmission Line Design Manual*; US Department of the Interior, Water and Power Resources Service: Denver, CO, USA, 1980.
35. Federal Emergency Management Agency. *Prestandard and Commentary for the Seismic Rehabilitation of Buildings (FEMA 356)*; Federal Emergency Management Agency: Washington, DC, USA, 2000.
36. Elnashai, A.S.; Di Sarno, L. *Fundamentals of Earthquake Engineering*; Wiley: New York, NY, USA, 2008.
37. Wang, G. A ground motion selection and modification method capturing response spectrum characteristics and variability of scenario earthquakes. *Soil Dyn. Earthq. Eng.* **2011**, *31*, 611–625. [[CrossRef](#)]
38. Villar-Vega, M.; Silva, V.; Crowley, H.; Yepes, C.; Tarque, N.; Acevedo, A.B.; Hube, M.A.; Gustavo, C.D.; María, H.S. Development of a fragility model for the residential building stock in South America. *Earthq. Spectra* **2017**, *33*, 581–604. [[CrossRef](#)]
39. Di Trapani, F.; Malavisi, M. Seismic fragility assessment of infilled frames subject to mainshock/aftershock sequences using a double incremental dynamic analysis approach. *Bull. Earthq. Eng.* **2019**, *17*, 211–235. [[CrossRef](#)]
40. Hosseini, R.; Rashidi, M.; Bulajić, B.Đ.; Arani, K.K. Multi-Objective Optimization of Three Different SMA-LRBs for Seismic Protection of a Benchmark Highway Bridge against Real and Synthetic Ground Motions. *Appl. Sci.* **2020**, *10*, 4076. [[CrossRef](#)]
41. Bulajić, B.Đ.; Bajić, S.; Stojnić, N. The effects of geological surroundings on earthquake-induced snow avalanche prone areas in the Kopaonik region. *Cold Reg. Sci. Technol.* **2018**, *149*, 29–45. [[CrossRef](#)]
42. Hatzigeorgiou, G.D.; Liolios, A.A. Nonlinear behaviour of RC frames under repeated strong ground motions. *Soil Dyn. Earthq. Eng.* **2010**, *30*, 1010–1025. [[CrossRef](#)]
43. Zahid, M.; Majid, T.; Faisal, A. Effect of repeated near field earthquake to the high-rise Rc building. *Aust. J. Basic Appl. Sci.* **2012**, *6*, 129–138.
44. Fazli, H.; Majid, T.A. Seismic Performance of 3 Storey Irregular Reinforced Concrete (RC) Frames Under Repeated Earthquakes. *Casp. J. Appl. Sci. Res.* **2013**, *2*, 60–65.
45. Faisal, A.; Majid, T.A.; Hatzigeorgiou, G.D. Investigation of story ductility demands of inelastic concrete frames subjected to repeated earthquakes. *Soil Dyn. Earthq. Eng.* **2013**, *44*, 42–53. [[CrossRef](#)]
46. Kennedy, R.P.; Cornell, C.A.; Campbell, R.; Kaplan, S.; Perla, H. Probabilistic seismic safety study of an existing nuclear power plant. *Nucl. Eng. Des.* **1980**, *59*, 315–338. [[CrossRef](#)]
47. Roy, S.; Kundu, C.K. State of the art review of wind induced vibration and its control on transmission towers. In *Structures*; Elsevier: Amsterdam, The Netherlands, 2021; Volume 29, pp. 254–264.